2021 43rd Annual International Conference of the
IEEE Engineering in Medicine & Biology Society (EMBC)
Oct 31 - Nov 4, 2021. Virtual Conference

# Robot-Assisted Electrical Impedance Scanning system for 2D Electrical Impedance Tomography tissue inspection

Zhuoqi Cheng[1*], Diego Dall'Alba[2], Paolo Fiorini[2] and Thiusius Rajeeth Savarimuthu[1]

*Abstract*— **The electrical impedance tomography (EIT) technology is an important medical imaging approach to show the electrical characteristics and the homogeneity of a tissue region noninvasively. Recently, this technology has been introduced to the Robot Assisted Minimally Invasive Surgery (RAMIS) for assisting the detection of surgical margin with relevant clinical benefits. Nevertheless, most EIT technologies are based on a fixed multiple-electrodes probe which limits the sensing flexibility and capability significantly. In this study, we present a method for acquiring the EIT measurements during a RAMIS procedure using two already existing robotic forceps as electrodes. The robot controls the forceps tips to a series of predefined positions for injecting excitation current and measuring electric potentials. Given the relative positions of electrodes and the measured electric potentials, the spatial distribution of electrical conductivity in a section view can be reconstructed. Realistic experiments are designed and conducted to simulate two tasks: subsurface abnormal tissue detection and surgical margin localization. According to the reconstructed images, the system is demonstrated to display the location of the abnormal tissue and the contrast of the tissues' conductivity with an accuracy suitable for clinical applications.**

## I. Introduction

Electrical Impedance Tomography (EIT) has become an important medical imaging modality and has been the focus of many researches in the past decades [1]. Different reconstruction algorithms have been developed to enable the visualization of the spatially distribution of electrical impedance within the area bounded by a set of electrodes. Since different tissues have distinguishable electrical properties, patient's physiological conditions and abnormal tissue regions can be reflected by the EIT images. For instance, EIT has been successfully applied to display preterm baby's lung filling [2], monitor regional cerebral edema [3], and early stage cancer diagnosis [4], [5]. Specifically, the malignant tumor is found to have generally higher conductivity or/and permittivity than its surrounding normal tissue [6]. Thus, the region of pathological tissue can be indicated by the impedance driven imaging.

The concept of electrical impedance based cancer detection has shown a lot of benefits for Robot-Assisted Minimally Invasive Surgery (RAMIS) [7], [8]. During a tumor resection operation, clear surgical margins are critical for the success of the surgery. Not adhering to the correct resection margins can lead to significantly higher rate of recurrence [9]. However, due to limited intra-operative perceptions, it is generally difficult for the surgeon to detect critical subsurface tissues and assess the surgical margin. Our previous studies have attempted to integrate the electrical bioimpedance sensing technology into a surgical robot [10], [11]. The electrical property is measured by a bipolar surgical forceps without introducing any dedicated external sensing probe to the scene. Since a bipolar sensing configuration is exploited, it is very sensitive to a local region and to the contacting area between the electrode and the tissue. Researchers from the Dartmouth college have developed a series of miniaturized EIT probes with multiple electrodes for prostate cancer detection during a minimally invasive surgery [12], [8]. Although the effectiveness has been demonstrated, the size constraints for entering a laparoscopic port limit the sensing capability of the probe. In another previous study, a Robot-Assisted Electrical Impedance Scanning (RAEIS) system has been proposed, showing enhanced impedance sensing capability and stability [13]. Through autonomous scanning on the tissue surface with the existing robotic forceps, the RAEIS system can detect non-homogeneous areas in the inspecting region.

Based on the RAEIS system described in [13], [14], this paper presents its application in a 2D EIT reconstruction. To the best of the authors' knowledge, this work is the first to perform the EIT measurement and reconstruction directly based on the existing instruments of a normal medical robotic system. Compared to the method presented in [13], the EIT imaging can provide more detailed visualization of the tissue subsection, which is believed to improve the efficacy for the surgery potentially. Experiments based on ex vivo tissues are designed and undertaken. The reconstructed EIT images demonstrates the capability of the proposed method for showing the location of abnormal tissue intra-operatively. The experimental results demonstrate the effectiveness of the proposed system and method by revealing the high sensitivity and specificity in locating a non-homogeneous region of the tissue phantom.

This paper is structured as follows. In Section II the system is described and mathematically formulated. Section III presents the experimental evaluation of the proposed system. The experimental results are presented in Section IV and Section V discusses and concludes the study.

## II. Methods

### A. Robot Assisted Electrical Impedance Scanning

The RAEIS system exploits a tripolar EBI sensing system which consists of a current source electrode (CSE), a

[1]Z. Cheng and T.R. Savarimuthu are with the Mærsk Mc Kinney Møller Instituttet, University of Southern Denmark, 5230 Odense, Denmark.

[2]D. Dall'Alba and F. Fiorini are with the Department of Computer Science, University of Verona, 37134 Verona, Italy.

*Corresponding author: Zhuoqi Cheng (email:zch@mmmi.sdu.dk)

voltage measurement electrode (VME) and a ground electrode (GND) [15]. Excitation electric current is injected to the tissue through the CSE, and the electric potentials at different surrounding locations are picked up through the VME. Meanwhile, the GND is made in a relatively bigger size and placed on a remote site of the tissue. Compared to the monopolar and bipolar configuration, a tripolar sensing configuration has a much lower sensitivity to the contact impedance, and thus the readings are more stable. Also, the tripolar configuration is less cumbersome than the tetrapolar which requires four electrodes for measurement.

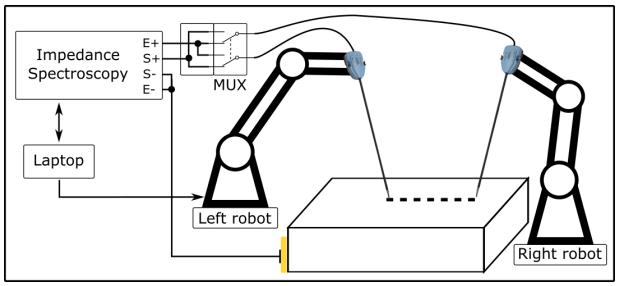


Fig. 1. The configuration of the RAEIS system.

In this study, the RAEIS system uses the tips of two surgical forceps as CSE and VME respectively. The GND electrode is made of a copper sheet and is used to reproduce the electric return pad which is essential in an electrosurgery. The position of each forceps is controlled by a separate robot. During the measurement, two electrodes are controlled to a series of positions on the tissue surface. As shown in Fig. 1, the impedance spectroscopy outputs an excitation current via channel $E+$ and $E-$, and measures a differential voltage from input between $S+$ and $S-$. The $E-$ and $S-$ are connected together to the GND electrode. An analog multiplexer (MUX) is used to switch the association between electrodes and the two forceps. The default setting of the MUX assigns the left forceps to work as the CSE and the right forceps as the VME. When the MUX is activated, the left forceps acts as the VME and the right forceps as the CSE. In addition, a laptop is used for coordinating the whole system including robots control, MUX activation and impedance measurements acquisition.

### *B. Electrical Impedance Tomography*

Since biological tissue is hard to be magnetized and the applied frequency for EIT is relatively low, the EIT model can be simplified as a static electric field. The current follows the Ohm's law:

$$J = \sigma E \tag{1}$$

where $\sigma$ is the conductivity and $E$ is the electric field. According to the continuity condition, the following equation is satisfied.

$$\bigtriangledown \cdot (\sigma \bigtriangledown \Phi) = 0 \tag{2}$$

which is also known as the Maxwell equation, describing the elliptic partial differential equation of the electric potential distribution $\Phi$ and the conductivity distribution $\sigma$.

To create the EIT imaging, it requires to solve the forward problem and the inverse problem iteratively [1]. The forward problem is to find out the electric potential in a defined domain given the boundary condition and the conductivity distribution in the domain. The inverse problem is a process to determine the conductivity distribution in the domain by knowing the boundary condition and the electrical potential distribution.

A method generally used for solving the partial differential equation (2) is the variational approach [16], which constructs a function and minimizes the residual. Here, the energy equation is defined as:

$$F(\Phi) = \frac{1}{2}\int_{\Omega} \sigma \bigtriangledown \Phi^2 d\Omega + \int_{\partial\Omega} J\Phi d\partial\Omega \tag{3}$$

The first term is the energy of an internal area $\Omega$, and the second term represents the energy introduced from the boundary $\partial\Omega$. The forward problem is normally solved using finite element approximation. Assuming that the field $\Omega$ is approximated by a collection of $K$ simplex elements with $N$ vertices, function $F(\Phi)$ in Eq. (3) can be written as

$$F(\Phi) = \sum_{k=1}^{K} \frac{1}{2}\int_{\Omega_k} \sigma^k \bigtriangledown \Phi^2 d\Omega + \int_{\partial\Omega} J\Phi d\partial\Omega \tag{4}$$

where $\sigma^k$ is the conductivity of an element $k$ in the mesh. Based on Eq. 4, the energy function of element $k$ can be further written as

$$F^k(\Phi) = \frac{1}{2}\sigma^k [\Phi^k]^T [Y^k][\Phi^k] \tag{5}$$

where $[\Phi^k]$ is a vector describing the potential of vertices for the element $k$, and $[Y^k]$ is a matrix describing the geometry of the element [17]. By solving Eq. (5), which is also known as the Laplacian equation, the electric potential at each node can be obtained.

To investigate the conductivity distribution in a field $\Omega$ (inverse problem), Green's theorem is used. If there is a current $I_\Phi$ injected into the tissue from electrode $i$, a voltage $\Phi_j$ can be measured at another position $j$. Also, when a current $I_\Psi$ is applied from electrode $j$, a voltage $\Psi_i$ can be measured at position $i$. According to Eq. (2), we have

$$\int_{\partial\Omega} \Phi\sigma \bigtriangledown \Psi \cdot d\partial\Omega = \int_{\Omega} \sigma \bigtriangledown \Phi \cdot \bigtriangledown \Psi d\Omega \tag{6}$$

The left part of Eq. (6) is the energy introduced from the boundary. Consider that the conductivity of one internal region changes from $\sigma$ to $\sigma + \Delta\sigma$, a redistribution of the current $I_\Phi$ associated with a change in potential from $\Phi$ to $\Phi + \Delta\Phi$ and from $\Psi$ to $\Psi + \Delta\Psi$ would happen. We assume that $\Delta\sigma$ is small enough, and the resultant $\Delta\Psi \ll \Psi$. Then Eq. (6) can be written as follows. Here, $S$ is the sensitivity matrix.

$$\Delta\Phi = -\int_{\Omega} \Delta\sigma \bigtriangledown \Phi \cdot \bigtriangledown \Psi d\Omega = S\Delta\sigma \tag{7}$$

The inverse problem is generally an ill-pose problems, different optimization approaches have been proposed and

used to approximate the result [18]. This is equivalent to seek the $\sigma$ which satisfy the following equation:

$$\Delta\sigma = argmin \parallel \Delta\Phi - L_1(\Delta\sigma) \parallel^2 + \alpha \parallel L_2(\Delta\sigma) \parallel^2 \quad (8)$$

where $L_1(\sigma)$ represents the update of computed boundary potentials, and $\alpha$ is the regularization parameter. $\Delta\Phi$ is the difference voltage input between the measurement on homogeneous material and the measurement of a specific condition. In this work, the Newton method is used to solve the following equations iteratively:

$$\begin{cases} \sigma_{n+1} = \sigma_n + \Delta\sigma_n \\ \Delta\sigma_n = (S_n^T S_n)^{-1}(S_n^T \Delta\Phi - \alpha I(\sigma_n - \sigma_{ref})) \end{cases} \quad (9)$$

### C. Measurement acquisition protocol

In this study, the EIT measurement is carried out along a line on the tissue surface in order to visualize the vertical section of tissue. As shown in Fig. 2(B), $\mathbf{N}$ equally spaced points along the line are defined. In addition, we denote the start point on the left as $\mathbf{P}_1$ and the end point on the right as $\mathbf{P}_N$. To avoid collision between two forceps, the following scanning protocol is implemented. Firstly, the left forceps acts as the CSE and the right forceps acts as the VME. The left forceps is controlled to contact a point $\mathbf{P}_i$ from left to right for injecting excitation current. After the CSE contacts the point $\mathbf{P}_i$, the right forceps measures voltage from $\mathbf{P}_{i+1}$ to $\mathbf{P}_N$. Subsequently, the CSE moves to the next point and the VME performs the measurements in sequence. After the above procedure is done, the work role of the left forceps and the right forceps switches. The right forceps injects excitation current from $\mathbf{P}_N$ to $\mathbf{P}_2$. For each CSE position at $\mathbf{P}_i$, the left forceps measures the voltage from $\mathbf{P}_{i-1}$ to $\mathbf{P}_1$. In total, the above procedure results to $\mathbf{N} \times (\mathbf{N} - 1)$ values as input to compute the tomography.

To ensure a good contact between the electrode and the tissue, a ramping motion as described in [13] is used. During this procedure, the VME is moved a step distance away from CSE and lifted up a small distance (3 mm). Then the VME moves downwards until it contacts the tissue, which can be detected by the change of impedance reading. Subsequently, the voltages at the corresponding positions are collected.

## III. Experiments

### A. Experimental setup

As shown in Fig. 2(A), the experimental setup includes two da Vinci robotic forceps as the CSE and VME respectively, and a piece of copper sheet (10 × 30 mm) as the GND. The GND electrode was attached to the right wall of the phantom. Two UR3 robot arms (Universal Robots A/S, Denmark) were involved to control the positions of two forceps. The forceps's wrists were all fixed, and both forceps tips were adjusted pointing downwards vertically. The robotics system was calibrated in terms of kinematics. By controlling the forceps tip to 10 predefined positions in the global coordinate manually, the transformation matrix from the tip of the forceps to base coordinate of the carrying robot were calculated. The re-projection error between two forceps are found to be 0.12 mm and 0.09 mm respectively.

The Eliko Quadra (Eliko Tehnoloogia Arenduskeskus OÜ, Estonia) was chosen as the impedance spectroscopy instrument. This device can provide simultaneous 15-frequency measurements from 1 kHz to 349 kHz in 1 ms. In addition, a very high measurement accuracy (0.1% repeatability error) was reported from the product datasheet.

### B. Experimental design

Two experiments were designed and carried out for evaluating the proposed system. Realistic phantom based on ex vivo porcine liver and muscle tissues were produced. Since muscle has a relatively higher conductivity than liver [19], it was used for simulating a cancer here.

The first experiment (Exp 1) is simulating a scenario where the proposed system was used for the detection of subsurface non-homogeneous tissue. As shown in Fig. 2(C), a big piece of liver tissue was first placed inside a container of 150×120×50 mm. Taking the left upper corner of the phantom as the origin, a slab of muscle (20×10×10 mm) was placed at (X = 55 mm to 65 mm) and (Y = 20 mm to 40 mm) on top of the liver tissue. Then another thin layer of liver tissue (about 5 mm) was covered on top of the muscle tissue. In Fig. 2(C), the top layer of liver tissue was lifted to show the location of the muscle tissue, while this top layer was laid down during the experiment. In the second experiment (Exp 2), another scenario was designed to simulate a surgical margin detection scenario. Fig. 2(D) shows the phantom for Exp 2. Both muscle and liver tissues were used. A small hole at (X = 55 mm to 65 mm, Y = 10 mm to 30 mm) was cut on the liver tissue, and the muscle slab was inserted into the hole. The location of the boundary was at Y = 30 mm. The surface of all the phantoms were made flat for the experiments to ensure optimal contact between the forceps and tissue.

During the experiments, the scanning was performed along the line X = 60 mm from Y = 10 mm to 65 mm. As indicated by the yellow dotted line in Fig. 2(A), 12 points were set given a step size of 5 mm. The scanning procedure (Fig. 2(B)) was conducted as described in Section II.C.

### C. Experimental data analysis

After the scanning on the phantom was completed, the EIT of the section view in Y-Z plane was generated. Matlab software (Mathworks Inc., U.S.) and the EIDORS library were used to solve the inverse problem and reconstruct the tomographic image. Specifically, the advanced inverse solver based on Andrea Borsic's Total Variation regularization was implemented [20]. In addition, the measurements on a piece of pure liver (Fig. 2(A)) were used as reference for the difference EIT reconstruction input. Based on the reconstructed tomographic image, the position accuracy and relative impedance values were analyzed in Section IV. In addition, the overall operating time was provided.

## IV. Results

During the experiments, the system was demonstrated to perform the required scanning procedure and generate an

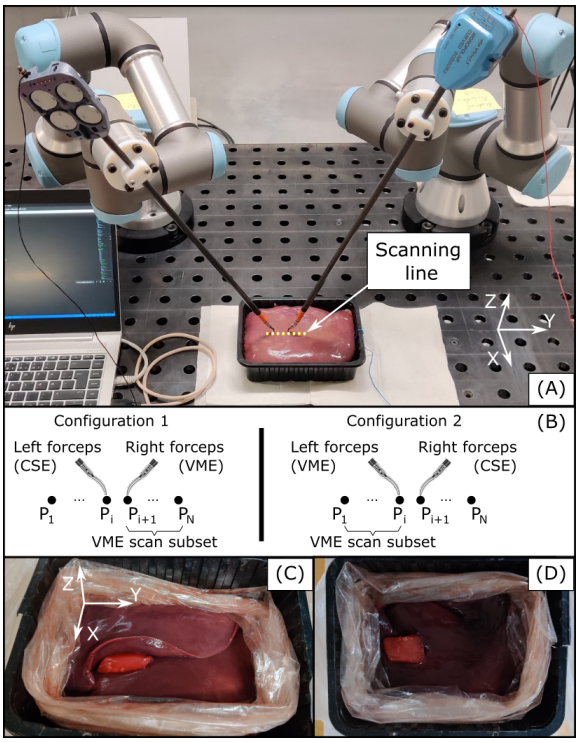


Fig. 2. (A) The experimental setup; (B) the measurement protocol; (C) the phantom designed for Exp 1 (the lifted top layer of liver is laid down on top of muscle during experiment); (D) the phantom designed for Exp 2.

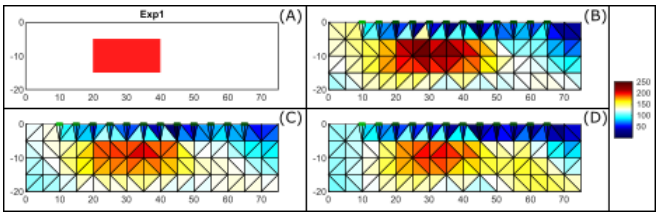


Fig. 3. (A) The ground truth subsection view of the phantom for Exp 1; (B)-(D) The reconstructed 2D EIT of Exp1 based on measurements with 1 kHz, 61 kHz and 349 kHz excitation frequency. (The dimensions are in $mm$.)

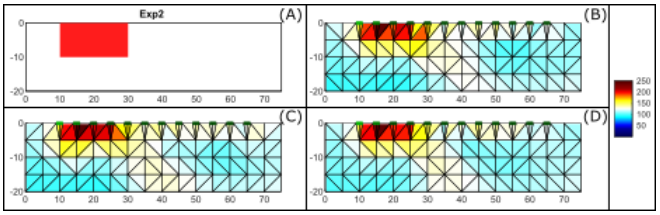


Fig. 4. (A) The ground truth subsection view of the phantom for Exp 2; (B)-(D) The reconstructed 2D EIT of Exp1 based on measurements with 1 kHz, 61 kHz and 349 kHz excitation frequency. (The dimensions are in $mm$.)

EIT image successfully. The scanning time for a 12 point linear pattern was 89 s, and the time for the tomographic reconstruction was 0.18 s.

The reconstructed 2D images in the Y-Z section plane are presented in Fig. 3 and Fig. 4. Specifically, the EIT reconstruction images show the region of 20 mm depth and 75 mm width (10 mm away from $\mathbf{P}_1$ and $\mathbf{P}_{12}$ respectively). In the reconstruction model, every electrode was made as a small plate (dark green on the top line) of 2 mm width to simulate the contacting area between the forceps and the tissue. In addition, since the reconstruction was done in 2D, the reconstructed images could show a relative conductivity instead of the exact conductivity of the tissues: red color scale represents regions with higher conductivity and blue color scale represents regions of lower conductivity.

Fig. 3(A) shows the expected subsection view of the phantom for Exp 1. The region in red represents the location of muscle inside the phantom. Fig. 3(B) shows the reconstructed results in three different frequencies (1 kHz, 61 kHz and 349 kHz). Considering that the reconstructed results in different frequencies look similar, we use only the results of 61 kHz as an example for analysis. According the results of Exp 1, the reconstructed tomography showed a region of higher conductivity from 5 mm to 15 mm in the depth, and from 20 mm to 45 mm in the width. Compared to the ground truths, the reconstruction image showed a correct depth but a 5 mm longer width (Fig. 3). The conductivity of the region of muscle (Y = 20 mm to 40 mm, Z = -5 mm to -15 mm) was computed to be 200.8±13.8. The conductivity of the rest region was found to be 109.7±38.3.

As for the reconstruction result of Exp 2 (Fig. 4), a region of higher conductivity was observed from 0 to 5 mm in the depth and from 10 mm to 30 mm in the width. This result indicated the location of muscle correctly in the width but 5 mm shorter in the depth. The conductivity of the muscle region (Y = 10 mm to 30 mm, Z = 0 mm to -10 mm) was computed, which is 188.4±36.7, and the conductivity of the rest region was found to be 122.2±12.2.

## V. Discussion and Conclusion

According to 2D tomography of the preliminary results, the RAEIS is demonstrated to be able to indicate the location of a non-homogeneous region under the surface or a margin between two materials. With respect to the location of muscle, the sensitivity of Exp 1 is 100%, and the specificity is 96%. For Exp 2, the sensitivity and specificity are 43.8% and 100% respectively. One possible reason for the low sensitivity in Exp 2 can be because the muscle was close to one side of the sensing array. Generally, EIT is reported to have relatively low spatial sensitivity compared to the other popular imaging methods [21]. Nevertheless, the reconstructed image of Exp 2 can accurately indicate the margin location between the muscle and liver, which is the goal of Exp 2. In addition, the ratio of the conductivity between muscle and liver are found to be 54.6% and 64.9% mm in both experiments respectively. This is similar to the information (∼60%) provided in [22].

In this study, we use 12 points during the impedance scanning which takes approximately 90 s. In practice, the number of scanning points and the distance between them can be adjusted according to the requirements. With fewer scanning points, the sensing accuracy and sensitivity may be reduced but a shorter scanning time could be obtained.

Given the encouraging results, the proposed system and method shows a great potential to be applied for various surgical procedures such as the localization of pathological tissue and assessment of surgical margin. More optimization activities will be performed to improve the system, and the sensor circuit will be made compatible with IEC60601-7 such as 1 mA current limit. Also, more realistic experimental evaluations will be conducted.

## ACKNOWLEDGMENTS

This study has been partially supported by the EUR commission ARS project (Grant No. H2020-ERC2017-3).

## REFERENCES

[1] B. H. Brown, "Electrical impedance tomography (eit): a review," *Journal of medical engineering & technology*, vol. 27, no. 3, pp. 97–108, 2003.

[2] A. Adler, J. H. Arnold, R. Bayford, A. Borsic, B. Brown, P. Dixon, T. J. Faes, I. Frerichs, H. Gagnon, Y. Gärber *et al.*, "Greit: a unified approach to 2d linear eit reconstruction of lung images," *Physiological measurement*, vol. 30, no. 6, p. S35, 2009.

[3] H. Li, R. Chen, C. Xu, B. Liu, M. Tang, L. Yang, X. Dong, and F. Fu, "Unveiling the development of intracranial injury using dynamic brain eit: an evaluation of current reconstruction algorithms," *Physiological measurement*, vol. 38, no. 9, p. 1776, 2017.

[4] V. Cherepenin, A. Karpov, A. Korjenevsky, V. Kornienko, A. Mazaletskaya, D. Mazourov, and D. Meister, "A 3d electrical impedance tomography (eit) system for breast cancer detection," *Physiological measurement*, vol. 22, no. 1, p. 9, 2001.

[5] J. Jossinet, E. Marry, and A. Montalibet, "Electrical impedance endotomography: imaging tissue from inside," *IEEE transactions on medical imaging*, vol. 21, no. 6, pp. 560–565, 2002.

[6] Z. Cheng, A. L. C. Carobbio, L. Soggiu, M. Migliorini, L. Guastini, F. Mora, M. Fragale, A. Ascoli, S. Africano, D. G. Caldwell *et al.*, "Smartprobe: a bioimpedance sensing system for head and neck cancer tissue detection," *Physiological measurement*, vol. 41, no. 5, p. 054003, 2020.

[7] G. Zhu, L. Zhou, S. Wang, P. Lin, J. Guo, S. Cai, X. Xiong, X. Jiang, and Z. Cheng, "Design of a drop-in ebi sensor probe for abnormal tissue detection in minimally invasive surgery," *Journal of Electrical Bioimpedance*, vol. 11, no. 1, pp. 87–95, 2020.

[8] A. Mahara, S. Khan, E. K. Murphy, A. R. Schned, E. S. Hyams, and R. J. Halter, "3d microendoscopic electrical impedance tomography for margin assessment during robot-assisted laparoscopic prostatectomy," *IEEE transactions on medical imaging*, vol. 34, no. 7, pp. 1590–1601, 2015.

[9] M. Rouanne, J. Rode, A. Campeggi, Y. Allory, D. Vordos, A. Hoznek, C.-C. Abbou, A. D. La Taille, and L. Salomon, "Long-term impact of positive surgical margins on biochemical recurrence after radical prostatectomy: ten years of follow-up," *Scandinavian journal of urology*, vol. 48, no. 2, pp. 131–137, 2014.

[10] Z. Cheng, D. Dall'Alba, S. Foti, A. Mariani, T. J. E. Chupin, D. G. Caldwell, G. Ferrigno, E. De Momi, L. S. Mattos, and P. Fiorini, "Design and integration of electrical bio-impedance sensing in surgical robotic tools for tissue identification and display," *Frontiers in Robotics and AI*, vol. 6, p. 55, 2019.

[11] K. L. Schwaner, D. Dall'Alba, Z. Cheng, L. S. Mattos, P. Fiorini, and T. R. Savarimuthu, "Robotically assisted electrical bio-impedance measurements for soft tissue characterization: a feasibility study," in *The Hamlyn Symposium on Medical Robotics*. The Hamlyn Centre, 2019, pp. 31–32.

[12] D. Meroni, C. C. Maglioli, D. Bovio, F. G. Greco, and A. Aliverti, "An electrical impedance tomography (eit) multi-electrode needle-probe device for local assessment of heterogeneous tissue impeditivity," in *2017 39th Annual International Conference of the IEEE Engineering in Medicine and Biology Society (EMBC)*. IEEE, 2017, pp. 1385–1388.

[13] Z. Cheng and T. R. Savarimuthu, "A novel robot assisted electrical impedance scanning system for subsurface object detection," *Measurement Science and Technology*, 2021.

[14] Z. Cheng, K. L. Schwaner, D. Dall'Alba, P. Fiorini, and T. R. Savarimuthu, "An electrical bioimpedance scanning system for subsurface tissue detection in robot assisted minimally invasive surgery," *IEEE Transactions on Biomedical Engineering*, 2021.

[15] S. Grimnes and O. G. Martinsen, *Bioimpedance and bioelectricity basics*. Academic press, 2011.

[16] V. Sarode, S. Patkar, and A. N. Cheeran, "Comparison of 2-d algorithms in elt based image reconstruction," *International Journal of Computer Applications*, vol. 69, no. 8, 2013.

[17] X. Zhang, "Investigation of 3d electrical impedance mammography systems for breast cancer detection," Ph.D. dissertation, University of Sussex, 2015.

[18] A. Adler and W. R. Lionheart, "Uses and abuses of eidors: an extensible software base for eit," *Physiological measurement*, vol. 27, no. 5, p. S25, 2006.

[19] D. Andreuccetti, "An internet resource for the calculation of the dielectric properties of body tissues in the frequency range 10 hz-100 ghz," *http://niremf. ifac. cnr. it/tissprop/*, 2012.

[20] A. Borsic, B. M. Graham, A. Adler, and W. R. Lionheart, "In vivo impedance imaging with total variation regularization," *IEEE transactions on medical imaging*, vol. 29, no. 1, pp. 44–54, 2009.

[21] E. K. Murphy, A. Mahara, and R. J. Halter, "Absolute reconstructions using rotational electrical impedance tomography for breast cancer imaging," *IEEE transactions on medical imaging*, vol. 36, no. 4, pp. 892–903, 2016.

[22] C. Gabriel, A. Peyman, and E. H. Grant, "Electrical conductivity of tissue at frequencies below 1 mhz," *Physics in medicine & biology*, vol. 54, no. 16, p. 4863, 2009.